Frontiers in Bioscience Landmark

Front. Biosci. (Landmark Ed) **2025**; 30(9): 42805
https://doi.org/10.31083/FBL42805

Original Research

LINC01605 Suppresses Esophageal Squamous Carcinogenesis by Regulating Squamous Cell Differentiation, Proliferation, and Migration

Xian Cheng[1], Xu Han[1], Haiyin An[1], Jialiang Fan[1], Junyi Li[1], Ting Xiao[1], Lin Feng[1], Shujun Cheng[1,*]

[1]State Key Laboratory of Molecular Oncology, Department of Etiology and Carcinogenesis, National Cancer Center/National Clinical Research Center for Cancer/Cancer Hospital, Chinese Academy of Medical Sciences and Peking Union Medical College, 100020 Beijing, China
*Correspondence: chengshj@cicams.ac.cn (Shujun Cheng)
Academic Editor: Alfredo Budillon
Submitted: 1 June 2025 Revised: 19 August 2025 Accepted: 9 September 2025 Published: 25 September 2025

Abstract

Background: Esophageal squamous cell carcinoma (ESCC) develops through a multistage process in which normal epithelium transitions into intraepithelial neoplasia and ultimately into invasive carcinoma. Elucidating the molecular changes and functional roles of key genes during this progression is critical for understanding the mechanisms underlying this malignant transformation. **Methods**: Transcriptomic profiles of 12 normal esophageal tissues, 5 intraepithelial neoplasia tissues, and 7 ESCC tissues were analyzed via microarray. Stage-specific transcriptomic changes were systematically compared to delineate the phenotypic evolution that occurs during carcinogenesis, with a particular focus on identifying pivotal genes that regulate the precancerous-to-malignant transition. The candidate gene *LINC01605* was further examined via the following approaches: (1) bioinformatics-based characterization of its tumor-associated functions using Genotype-Tissue Expression Project (GTEx) normal tissue and The Cancer Genome Atlas Program (TCGA) ESCC transcriptome; (2) functional validation in ESCC cell lines in which the gene was silenced or overexpressed *in vitro*; and (3) mechanistic exploration of RNA-binding partners via streptavidin bead-based RNA pull-down assays. **Results**: Multistage transcriptomic analysis revealed the progressive acquisition of cancer hallmarks during ESCC development. The transition from precancerous lesions to invasive carcinoma was characterized by epithelial dedifferentiation, extracellular matrix remodeling, and angiogenesis. *LINC01605*, which is a long noncoding RNA (lncRNA), was downregulated during this transition. GTEx revealed that *LINC01605* was specifically expressed in the squamous epithelium of the esophagus and that its expression was negatively correlated with histological grade in the TCGA-ESCC dataset. Samples with high *LINC01605* expression and those with low *LINC01605* expression in the TCGA dataset exhibited significant functional differences in epithelial cell differentiation, proliferation, and migration, as well as in the extracellular matrix. Knocking down *LINC01605* increased proliferation and migration in both the normal immortalized esophageal epithelial cell line NE3 and the ESCC cell line KYSE180. Conversely, the overexpression of *LINC01605* isoforms suppressed these malignant phenotypes. RNA pull-down revealed potential interactions between LINC01605 and aurora kinase B (AURKB), which are components of the chromosomal passenger complex (CPC), suggesting its involvement in regulating the cell cycle. **Conclusion**: *LINC01605* functions as a tumor suppressor in ESCC by maintaining squamous cell differentiation and inhibiting proliferation and migration. *LINC01605* downregulation facilitates malignant transformation during esophageal carcinogenesis.

Keywords: esophageal squamous cell carcinoma; LINC01605; RNA, long noncoding; anaplasia; carcinogenesis

1. Introduction

According to GLOBOCAN 2022 data, 510,000 new cases of esophageal cancer are diagnosed annually worldwide, with 43.8% diagnoses occurring in China. Esophageal squamous cell carcinoma (ESCC) represents the predominant histological subtype of esophageal cancer, accounting for approximately 85% of all esophageal malignancies worldwide and 95.5% of cases in China [1]. The current first-line therapy for treating advanced ESCC involves programmed cell death protein-1 (PD-1) inhibitors combined with chemotherapy; however, long-term survival rates remain suboptimal, with a median overall survival time of 15.3 months and a 3-year survival rate of only 25.6% [2]. Early detection and intervention remain critical for improving patient outcomes. Elucidating the molecular changes that occur during ESCC progression, particularly identifying key drivers of the transition from nonmalignant precancerous lesions to invasive carcinoma, is essential for developing early intervention strategies and discovering novel therapeutic targets.

Over the past decade, large-scale genomic sequencing studies of ESCC have been conducted worldwide. Early sequencing efforts focused primarily on comparative genomic analyses involving tumor tissues and adjacent normal tissues and identified high-frequency somatic changes in genes such as *TP53*, *CDKN2A*, *FAT1*, *NOTCH1*, *PIK3CA*, *KMT2D*, and *NFE2L2* as drivers of esophageal squamous carcinogenesis [3]. The progression from normal esophageal epithelium to ESCC occurs over decades, and esophageal squamous intraepithelial neoplasia (EIN)

has been recognized as the established precursor lesion [4]. Liu *et al*. [5] and Chen *et al*. [6] demonstrated substantial genomic similarities between EIN and ESCC via comparative sequencing analyses that included single nucleotide variants (SNVs) and copy number variations (CNVs). Their studies revealed that clonal mutations that are prevalent in ESCC tissues are already abundant in EIN tissues, indicating that esophageal carcinogenesis initiates as a heterogeneous clonal evolution process that begins in the early precancerous stage. Subsequent multistage analyses by Chang *et al*. [7] revealed that dynamic clonal shifts occur during malignant progression, notably a transition from *NOTCH1*-mutant dominant clones to *TP53*-mutant dominant populations. Their work identified biallelic *TP53* inactivation as the earliest event that drives the formation of premalignant lesions, whereas later stages of carcinogenesis were driven by the accumulation of CNVs and Apolipoprotein B mRNA Editing Catalytic Polypeptide-like (APOBEC)-associated mutagenesis following *TP53* mutation. However, the key factor that leads to the transformation of EIN into ESCC remains unclear.

Recent technological advances over the past three years have enabled the performance of multiple transcriptomic studies to investigate multistage esophageal squamous carcinogenesis. Chen *et al*. [8] used spatial transcriptomic profiling to demonstrate that abnormal epithelial cell interactions in the basal layer of precancerous lesions promote esophageal tumorigenesis by coordinating epithelial–mesenchymal transition (EMT) and the acquisition of hyperproliferative phenotypes. These interactions are mediated by the TP53-TP63/ΔNP63-EFNB1-EPHB4 signaling axis. Additionally, Chang *et al*. [9] performed single-cell transcriptomic sequencing of multistage lesions and delineated an evolutionary trajectory of the epithelial subpopulation. A distinct highly proliferative epithelial cluster undergoes progressive dedifferentiation during precancerous progression, acquiring invasive characteristics through Jagged1 (JAG1)-NOTCH1-mediated crosstalk with fibroblasts. This interaction establishes a protumorigenic epithelial–fibroblast niche that remodels extracellular matrix components and reprograms immune cell infiltration patterns, ultimately driving malignant transformation.

Notably, these studies identified functionally relevant genes that exhibit aberrant expression patterns during esophageal carcinogenesis. Epithelial-specific dysregulation of deltex E3 ubiquitin ligase 3L (*DTX3L*), along with stromal overexpression of bone marrow stromal cell antigen 2 (*BST2*) [10], has been mechanistically associated with malignant transformation. However, emerging evidence highlights that ESCC development represents a highly heterogeneous evolutionary process that involves the dynamic interplay between subclones of epithelial cells and microenvironmental components and that this interplay begins in the precancerous stage. While numerous genomic and transcriptomic aberrations have been identified, the critical determinants that enable high-grade intraepithelial neoplasia to cross the malignant threshold, particularly the master regulators that orchestrate this phenotypic transition, remain incompletely characterized.

2. Materials and Methods

2.1 Sample Collection and Processing

A total of 29 prospectively collected tissue samples from 12 treatment-naïve ESCC patients and dysplastic patients were analyzed in this study. The cohort included five dysplastic lesions with matched incisional margin tissues and distal normal mucosa that were obtained via endoscopic resection procedures and seven paired ESCC tumor and normal tissue samples at the Cancer Hospital of Chinese Academy of Medical Sciences (Beijing, China). All the samples were immediately preserved in RNAlater™ Stabilization Solution (Cat#AM7021, Thermo Fisher Scientific, Waltham, MA, USA) for $\geq$12 hrs at 4 °C, followed by long-term storage at –80 °C.

2.2 RNA Extraction and Microarray Analysis

Total RNA isolation was performed with the RNeasy Micro Kit (Cat#74104, Qiagen, Germantown, MD, USA) following the manufacturer's protocols for processing frozen tissues. RNA quantity and quality were systematically assessed using dual-platform validation: concentration measurements were performed with a NanoDrop2000 spectrophotometer (Thermo Fisher Scientific, Waltham, MA, USA), and integrity evaluation was performed with the Agilent 2100 Bioanalyzer System (Agilent Technologies, Santa Clara, CA, USA). All the RNA samples met stringent quality control criteria (total yield >2 µg; RNA integrity number [RIN] >6.0) prior to microarray processing. The 29 qualified RNA samples were hybridized to Agilent SurePrint G3 Human GE 8 × 60 K Microarray slides (Design ID: G4851B, Agilent Technologies, Santa Clara, CA, USA) following standardized manufacturer protocols. Post hybridization arrays were scanned at 3-µm resolution using the Agilent SureScan Microarray Scanner (G2600D, Agilent Technologies, Santa Clara, CA, USA), and fluorescence signal quantification was performed with Agilent Feature Extraction Software (v10.5.1.1, Agilent Technologies, Santa Clara, CA, USA). The raw intensity data were normalized with Agilent GeneSpring GX 12.0 software (Agilent Technologies, Santa Clara, CA, USA) with quantile normalization baseline transformation. Subsequent analysis focused on 18,681 probes corresponding to annotated human genes.

2.3 R Packages and Data Resources for Transcriptomic Analysis

The data used for the analyses described in this manuscript were obtained from the Genotype-Tissue Expression Project (GTEx) Portal on 09/15/2023 and the log2(FPKM+0.001)-transformed transcriptome data of

pancancer cohorts in the The Cancer Genome Atlas Program (TCGA) and normal tissues of normal tissues in the GTEx project, which were uniformly processed by the UCSC Toil RNA-seq Recompute Compendium without computational batch effect adjustment, were downloaded from UCSC Xena. Differential gene expression analysis was performed using the *gtools* R package (Version3.8.1) to identify statistically significant changes in transcription patterns. Pathway enrichment and tumor biology characterization were conducted with the gene set variation analysis (*GSVA*) package. Functional annotation of the gene ontology (GO) terms was systematically explored using the *clusterProfiler* R package (Version 2.99.2). The corresponding GO terms of cancer hallmarks were found in the literature [11]. Pairwise comparative analyses between the normal (N), dysplastic (D), and tumor (T) groups were performed using two-tailed Student's *t* tests. To ensure biological relevance while maintaining analytical rigor, we established stringent differential expression criteria: genes with a p value < 0.05 and absolute log2(fold change (FC)) >1.2 in any intergroup comparison were classified as differentially expressed genes (DEGs).

2.4 Cell Lines and Cell Culture

ESCC cell lines used in this study were originally sourced from the Japanese Collection of Research Bioresources (JCRB Bank, Osaka, Japan). The Immortalized esophageal epithelial cell lines NE2 and NE3 were a generous gift from Prof. Tong Tong (State Key Laboratory of Molecular Oncology, National Cancer Center/National Clinical Research Center for Cancer/Cancer Hospital, Beijing, China). All cellular materials have been preserved and routinely maintained in our laboratory's cell culture facility according to standard protocols. All the cell lines that were used in this study were confirmed by STR profiling and tested negative for mycoplasma. The ESCC cell lines were cultured in RPMI-1640 medium (Gibco, # C11875500CP, Thermo Fisher Scientific, Waltham, MA, USA) supplemented with 10% heat-inactivated fetal bovine serum (FBS; Life Technologies, Grand Island, NY, USA) in 5% CO_2 at 37 °C. Immortalized esophageal epithelial cell lines (NE2 and NE3) were maintained in a 1:1 mixture of defined Keratinocyte-SFM (dKSFM; Gibco, #17005-042, Thermo Fisher Scientific, Waltham, MA, USA) and Epithelial Cell Medium (Epife; Gibco, #A10008-01, Thermo Fisher Scientific, Waltham, MA, USA), and optimal growth conditions for promoting normal epithelial phenotypes were maintained.

2.5 Rapid Amplification of cDNA Ends (RACE) Analysis

The 5′ and 3′ ends of cDNA were experimentally resolved using the SMARTer® RACE 5′/3′ Kit (Cat# 634859, Takara Bio, Mountain View, CA, USA) following standardized protocols. In brief, total RNA from NE3 cells was treated with RNase-free DNase I (Cat#2270A, Takara Bio, Mountain View, CA, USA) to eliminate genomic DNA contamination. Then, 3′ RACE-ready cDNA was synthesized from 1 μg of RNA using 3′-CDS Primer A. Next, 5′ RACE-ready cDNA was generated with the 5′-CDS Primer and SMARTer II A Oligo. Gene-specific RACE primers were designed on the basis of the NCBI reference sequence (NR_121620.2) and microarray probe alignment; the primers were designed to have an optimal Tm, and secondary structure formation was avoided. The Advantage® GC 2 PCR Kit (Cat#639119, Takara Bio, Mountain View, CA, USA) was used to address challenges related to the template GC content (65–75%). Then, amplified bands were separated by 1.5% agarose gel electrophoresis, extracted from the gels (Qiagen Gel Extraction Kit), cloned, inserted into the pEASY®-T1 Cloning Vector (Cat#CT101-01, TransGen Biotech, Beijing, China), and subjected to bidirectional Sanger sequencing (10+ clones per band).

2.6 Plasmid Construction

The transcript-specific primers were designed on the basis of 5′/3′ RACE-defined terminal sequences of full-length *LINC01605* transcripts. The EcoRI and XhoI restriction site sequences were added to the 5′ ends of the forward primer and reverse primer, respectively. The full-length LINC01605 transcript sequence without the poly A tail was amplified from cell-derived cDNA by Polymerase Chain Reaction (PCR), and then, it was cloned and inserted into the EcoRI/XhoI sites of the mammalian expression vectors pcDNA3.1(+) and pcDNA3.1(–) (Cat#V790-20 and Cat#V795-20, Invitrogen, Carlsbad, CA, USA) to generate the pcDNA3.1(+)-LINC01605 vector and pcDNA3.1(–)-LINC01605.

2.7 Transfection Assays

LINC01605-specific siRNA and scrambled negative control siRNA were purchased from Invitrogen (Carlsbad, CA, USA). The *LINC01605* plasmid was constructed as described above. Cells were seeded in 6-well plates in antibiotic-free medium, and after 24 hrs of incubation, the cells had reached 50% (siRNA) or 80% (plasmid) confluence. Transfection complexes containing 100 nM siRNA or 2 μg of plasmid and Lipofectamine™ 3000 (L3000001, Thermo Fisher Scientific, Waltham, MA, USA) were prepared in Opti-MEM® (Gibco, #31985070, Thermo Fisher Scientific, Waltham, MA, USA) at a 1:2 (v/v) lipid:nucleic acid ratio. The complexes were then added dropwise to the cells, the cells were incubated for 6 hrs, and then, the medium was replaced with complete medium. The knockdown/overexpression efficiency was assessed 48 hrs posttransfection via quantitative real-time PCR (qRT–PCR) with TaqMan™ assays, and gene expression was normalized to GAPDH expression. Functional assays were conducted between 24 and 72 hrs posttransfection.

2.8 Cell Proliferation Assays

Cell proliferation rates were measured with the Cell Counting Kit-8 (CCK-8) assay or the xCELLigence Real-Time Cell Analyzer (RTCA)-MP (Acea Biosciences/Roche Applied Science, San Diego, CA, USA) system. KYSE180 and KYSE30 cells were transfected with the pCDNA3.1(+)-*LINC01605* plasmid or control plasmid, and KYSE180 and NE3 cells were transfected with LINC01605-targeting siRNA or negative control siRNA. After 24 hrs, the cells were seeded in 96-well plates at a concentration of 2000 cells/100 µL of culture medium per well. For assays involving the xCELLigence Real-Time Cell Analyzer (RTCA)-MP system, the machine automatically measures electrical impedance every 15 min to determine cell proliferation in real time. At the end of the experiment, the proliferation rate determined by measuring the electrical impedance was plotted as a cell index ± SD. For the CCK-8 assay, at 4 hrs, 24 hrs, 48 hrs, 72 hrs, 96 hrs, and 120 hrs after seeding, the medium in one group of wells was replaced with 100 µL of medium supplemented with 10% CCK-8 (Cat#CK04, Dojindo, Kumamoto, Japan) per well, and the cells were cultured for 2 hrs at 37 °C. The degree of cell proliferation was determined by measuring the absorbance of each well with a 490-nm measurement filter and a 630-nm reference filter using a microplate reader SynergyTM HTX (BioTek, Winooski, VT, USA).

2.9 Transwell Migration Assays

After being transfected with the *LINC01605* plasmid or LINC01605-targeting siRNA for 48 hrs, the cells were resuspended in serum-free medium and added to the upper chamber of a Transwell plate with 6.5 mm-diameter chambers and an 8.0-µm pore size (Cat#3422, Corning, Corning, NY, USA). For KYSE180 cells, 3~4 $\times$ 10^5cellswere seeded in each chamber, the lower chambers were filled with culture medium supplemented with 40% FBS, and the plates were cultured for 24 hrs. For KYSE30 cells, 1 $\times$ 10^5 cells were seeded in each chamber, the lower chambers were filled with culture medium supplemented with 30% FBS, and the plates were cultured for 10 hrs. For NE3 cells, 1 $\times$ 10^5 cells were seeded in each chamber, the lower chambers were filled with culture medium supplemented with 20% FBS, and the plates were cultured for 12 hrs. Each chamber was observed under a microscope, and the cells in nine fields of view in a nine-grid pattern were counted.

2.10 RNA Isolation, Reverse Transcription PCR (RT-PCR) Analysis and Real-time PCR

Total RNA was extracted from the ESCC cell lines and esophageal epithelial tissues with the TRIzol reagent (Cat# 15596018CN, Invitrogen, Carlsbad, CA, USA). Two micrograms of RNA were reverse transcribed into cDNA with random primers and M-MLV reverse transcriptase (Cat#M1701, Promega, Madison, WI, USA) according to the manufacturer's instructions. qRT–PCR was conducted with the SYBR Premix Ex Taq^{TM} II (Tli RNase H Plus) kit (Cat#RR820A, TaKaRa, Kyoto, Japan) and an Applied Biosystems V7000 instrument (Thermo Fisher Scientific, Waltham, MA, USA). GAPDH was used as an internal reference for normalization. The PCR conditions were as follows: 30 s at 95 °C for preincubation and then 5 s at 95 °C and 31 s at 60 °C for 40 amplification cycles. The primers that were used were as follows:

LINC01605 forward: AAGCAGAAGACCCTCCTCAAAG.

LINC01605 reverse: GATCCAAGCACAGTCCCAGAA.

GAPDH forward: GAGAAGGCTGGGGCTCATTT.

GAPDH reverse: AGTGATGGCATGGACTGTGG.

2.11 RNA Pull-down Assay

An RNA pull-down assay was performed as previously described [12]. The pCDNA3.1(+)-*LINC01605* and pcDNA3.1(–)-*LINC01605* plasmids were linearized with the restriction enzymes corresponding to the sequences that were added to the 3′ end of the template DNA for vector cloning to conduct the *in vitro* transcription of LINC01605 and its antisense sequence. *In vitro* transcription was conducted using the MEGAscript T7 Kit (Cat#AM1333, Ambion, Austin, TX, USA). Total RNA was labeled with biotin-16-UTP (Cat#AM8452, Ambion, Austin, TX, USA) during transcription and purified with the MEGAclear Kit (Cat#AM1908, Ambion, Austin, TX, USA) according to the manufacturer's instructions. Five micrograms of biotinylated RNA were heated to 95 °C for 2 min, cooled on ice for 3 min, and then incubated at room temperature for 30 min. RNA were mixed with 500 µg of precleared NE3 cell extracts in binding buffer (10 mM HEPES pH 7.0, 50 mM KCl, 10% glycerol, 1 mM EDTA, 1 mM DTT, 0.5% Triton X-100) supplemented with tRNA (0.1 µg/µL), heparin (0.5 µg/µL) and RNasin (1 unit), and then, the mixtures were incubated at room temperature for 30 min. Fifty microliters of washed streptavidin agarose beads (Cat#SA10004, Invitrogen, Carlsbad, CA, USA) were added to each binding reaction, and the reactions were further incubated at room temperature for 15 min. The beads were washed five times with binding buffer and boiled in 1 $\times$ loading buffer for 10 min. The retrieved proteins were subjected to SDS–PAGE and further visualized by silver staining or immunoblotting.

2.12 Flow Cytometry

KYSE30 cells were transfected with the pCDNA3.1(+)-*LINC01605* recombinant plasmid or pCDNA3.1(+)-NC plasmid. 24 hrs after transfection, the cells were incubated in serum-free RPMI-1640 medium for 24 hrs to induce cell cycle arrest at the G0/G1 phase in order to synchronize the cell cycle. After the cells were serum starved, the medium was replaced with complete medium supplemented with 10% fetal bovine serum (FBS; Gibco, Thermo Fisher Scientific, Waltham, MA, USA)

and cultured for an additional 24 hrs to allow proliferation to resume. The cells were digested with trypsin, washed twice with ice-cold phosphate-buffered saline (PBS; 1000 ×g, 5 min), and resuspended in 1 mL of PBS. The cell suspensions were vortexed gently while 3 mL of ice-cold 70% ethanol (prechilled to –20 °C) was slowly added in a dropwise manner. Fixed cells were stored at 4 °C for ≥1 hr. Fixed cells were washed with PBS, treated with 2 µL of RNase A (0.25 mg/mL; Thermo Fisher Scientific, Waltham, MA, USA) in 200 µL of PBS, and incubated at 37 °C for 30 min to eliminate RNA interference. The cells were stained with 50 µg/mL PI solution (Cat#P4846, Sigma–Aldrich, St. Louis, MO, USA) supplemented with 0.1% Triton X-100 for 15 min in the dark. The samples were filtered through a 40-µm cell strainer and analyzed using a BD FACSCanto™ II flow cytometer (BD Biosciences, San Jose, CA, USA) with excitation at 488 nm and emission detection at 610 nm.

2.13 Statistical Analysis

Unless otherwise specified, all comparative tests in this study were performed using unpaired *t*-tests implemented in GraphPad Prism 7.0 (San Diego, CA, USA). A threshold of $p < 0.05$ was considered statistically significant.

3. Results

3.1 Multistage Transcriptomic Profiling Reveals Stepwise Acquisition of Cancer Hallmarks During Esophageal Squamous Carcinogenesis

We performed expression microarray profiling of 29 clinical samples, including 7 ESCC tissue (T) and paired adjacent normal tissue (N) samples from 7 patients with advanced ESCC and 5 severe dysplasia tissue (D), 5 dysplastic margin tissue (Q), and 5 paired normal tissue (N) samples from 5 patients with dysplasia. A total of 18,681 probes corresponding to 13,453 genes positively recognized their targets across the cohort.

Guided by Hanahan and Weinberg's seminal framework of cancer hallmarks [13], we performed GSVA [14] to map hallmark activation patterns (Fig. 1A). Transcriptomic profiling revealed that despite the lack of malignant transformation, severe dysplasia tissue samples already exhibited activation of four core oncogenic hallmarks: replicative immortality, sustained proliferative signaling, evasion of growth suppression and genome instability and mutation. Notably, these precancerous lesions maintained near-normal expression patterns of genes related to energy metabolism reprogramming, apoptosis resistance, and angiogenesis activation. Hallmarks of advanced malignancy, including tissue invasion/metastasis, tumor-promoting inflammation, and immune evasion, demonstrated progressive activation from dysplasia to carcinoma. While incipient activation trends were observed in the dysplasia tissues samples, the magnitudes of these trends remained orders of magnitude below the levels observed in carcinomas. These findings are consistent with the results of previous multiomics studies, establishing that in early stages of esophageal carcinogenesis, epithelial-intrinsic alterations are prioritized, whereas progression to invasive carcinoma requires microenvironmental reprogramming and interactions with the microenvironment.

To identify the molecular determinants of the precancerous-to-invasive carcinoma transition, we performed pairwise *t* tests to compare gene expression profiles among normal, severe dysplasia, and ESCC tissue samples (n = 29). This analysis revealed 2345 differentially expressed genes (DEGs) with significant intergroup differences in expression ($p < 0.05$, $|\log2FC| > 1.2$) most of these genes exhibited patterns of progressively dysregulated expression that were consistent with the findings of previous multistage carcinogenesis reports (Fig. 1B). Notably, 568 genes (271 downregulated, 297 upregulated) exhibited stage-specific changes in expression; these genes maintained stable expression during the progression from normal to dysplastic tissue but exhibited significant dysregulation during the carcinoma stage. We hypothesize that these genes may be critical drivers of the precancerous lesion-to-carcinoma transition. Functional enrichment analysis revealed that genes that were downregulated in specific stages were enriched mainly in metabolic regulation, epithelial differentiation, and keratinization functions (Fig. 1C), whereas genes that were upregulated were associated with extracellular matrix reorganization, angiogenesis and several metabolic processes (Fig. 1D). These findings are consistent with our hallmark progression analysis and confirm the findings of previous transcriptomic studies demonstrating that squamous cell dedifferentiation and ECM remodeling are pivotal events in malignant transformation.

3.2 LINC01605 Expression is Associated With Squamous Cell Differentiation in ESCC

Previous multi-stage studies on esophageal carcinogenesis and our chip-array data consistently indicated that dedifferentiation and ECM remodeling critically drives esophageal cancer development. Concurrently, long noncoding RNA (lncRNA)—noted for high tissue specificity and roles in tissue cell differentiation—suggested a potential link to this process [15]. Thus, we investigated whether the 567 genes dynamically unchanged from normal to precancerous stages but altered during the precancerous-to-cancerous transition included lncRNAs. We found that there were 30 lncRNAs with significantly altered expression during the progression from precancerous lesions to cancer along with protein-coding mRNAs. Among these, LINC01605 ranked among the top 5 most differentially expressed lncRNAs ($p < 0.05$ by unpaired *t*-tests, FC = 4.5). The RefSeq database records (versions before 2020) revealed two nonoverlapping transcripts of the

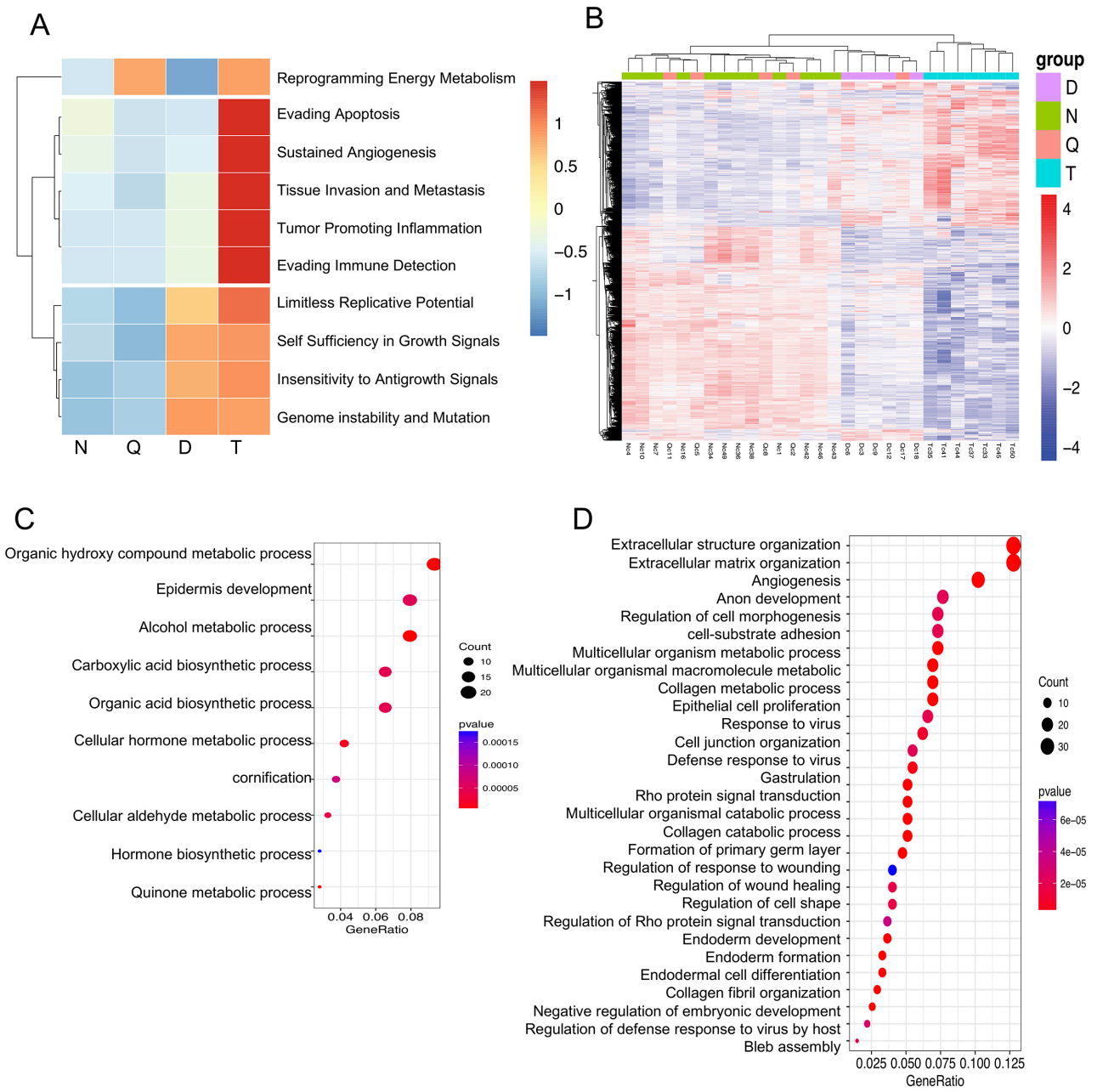

Fig. 1. Differentially expressed genes and transcriptomic features of each stage of esophagus carcinogenesis. (A) Heatmap showing the hallmark scores of each group of tissues. (B) Heatmap showing the changes in the expression of 2345 dysregulated genes between each pair of the N, D, and T groups. (C) Functional enrichment analysis of genes that were downregulated in specific tumor stages relative to their expression in high-grade dysplasia and normal tissues. (D) Functional enrichment analysis of genes that were upregulated in specific tumor stages relative to their expression in high-grade dysplasia and normal tissues. N, normal tissues; Q, dysplastic margin tissues; D, severe dysplasia tissues; T, esophageal squamous cell carcinoma tissues.

LINC01605 gene locus. Probe sequence alignment confirmed that the differentially expressed transcript that was detected in our microarray corresponded to the longer isoform NR_121620.2. We re-examined LINC01605 expression in the original chip cohort, comparing paired normal and precancerous lesion tissues from each patient. Paired comparative analysis of the microarray samples confirmed that this isoform was marginally upregulated in 5/5 severe dysplasia samples but obviously downregulated in 5/7 ESCC samples (Fig. 2A). Given the limited sample size of our microarray cohort, we extended the dataset to the GTEx [16] and TCGA transcriptomic datasets to validate the LINC01605 expression pattern. GTEx data revealed squamous epithelium-specific LINC01605 expression, with a Tau index of gene tissue specificity of 0.91. Genes with a tau index close to 1 are more specifically

expressed in one tissue [17]. Robust LINC01605 expression in the esophageal mucosa but no LINC01605 expression in the gastroesophageal junction mucosa and the vast majority of other normal tissues (Fig. 2B). According to TCGA-ESCA data, LINC01605 expression was significantly downregulated in carcinomas compared with normal tissues when esophageal adenocarcinoma (EAC) and ESCC data were considered together. However, subtype-specific stratification demonstrated that LINC01605 expression was preserved in ESCC vs. GTEx normal samples, although it was markedly downregulated in EAC samples (Fig. 2C). This finding was inconsistent with the findings of our small-sample microarray that revealed ESCC-specific downregulation of LINC01605. Given the squamous epithelium-specific expression pattern of LINC01605 and its regulation in conjunction with genes that are involved in epithelial morphogenesis/keratinization, we hypothesized that LINC01605 may be involved in regulating differentiation. When stratified by histological grade, the LINC01605 expression level was negatively correlated with tumor grade ($p < 0.05$ by one-way ANOVA test), with poorly differentiated tumors (G3) exhibiting marked LINC01605 downregulation compared with normal epithelium ($p = 0.0077$) (Fig. 2C), mirroring the dedifferentiation trajectory that is observed during malignant progression.

To confirm the differential expression of LINC01605 between normal and neoplastic squamous epithelial tissues, we performed qRT-PCR analysis on 10 ESCC cell lines and 2 immortalized normal esophageal squamous cell lines. Compared with all 10 ESCC lines, the immortalized normal cells lines exhibited significantly greater LINC01605 expression ($p < 0.001$) (Fig. 2D). Further validation in 10 paired ESCC and normal tissue samples revealed that LINC01605 expression was reduced by more than 2-fold in 4/10 cancer tissues compared with matched normal tissues (Fig. 2E). Notably, this reduction occurred in 4 out of 5 poorly differentiated ESCC cases. And consistent with prior TCGA data, no significant difference in expression was observed between normal and adjacent tissues overall. Despite heterogeneous LINC01605 downregulation across samples, the evidence, including squamous cell-specific expression patterns, differentiation-grade correlations and high expression in normal cell lines, collectively demonstrated that LINC01605 is associated with esophageal epithelial cell differentiation.

3.3 LINC01605 Potentially Regulates Phenotypic Transitions During Esophageal Epithelial Cell Differentiation

As previously reported, the dedifferentiation process plays a key role in the carcinogenesis of esophageal squamous epithelium. We investigated which phenotype of ESCC cells was affected by *LINC01605*, which is a gene that is related to the differentiation of the esophageal epithelium. We analyzed the differentially expressed genes in samples with the top 25% and bottom 25% of LINC01605 expression levels in the TCGA-ESCC transcriptome dataset. Genes with significantly greater expression ($p < 0.05$, $|FC| > 2$) in samples with higher levels of LINC01605 expression were significantly enriched in Gene Ontology terms including epidermis development, keratinocyte differentiation, and epidermal cell differentiation (Fig. 3A). These findings are consistent with the observed correlation between LINC01605 expression levels and tumor differentiation grade, further supporting the functional involvement of LINC01605 in esophageal squamous cell differentiation. Esophageal epithelial cell differentiation is a coordinated process that involves morphological restructuring, molecular reprogramming, and functional specialization, and it is characterized by decreased proliferative activity, terminal differentiation, tight junction formation, and reduced migratory capacity [18]. This program is pathologically reversed during dedifferentiation in carcinogenesis. Gene whose expression were coregulated with LINC01605 expression were also showed significant enrichment in functional categories related to epithelial cell proliferation, migration, and adhesion, as well as cell-matrix remodeling, which are all phenotypic hallmarks of dedifferentiation. In contrast, genes whose expression was relatively high in the samples with low LINC01605 expression were enriched in the regulation of membrane potential and synapse organization, which are biological processes that are typically associated with neuronal physiology (Fig. 3B). The phenotypic relevance of these neuro-related pathways in ESCC remains to be elucidated.

To characterize the potential function of *LINC01605* more accurately using genes that encode functional proteins, we identified the top 20 genes whose expression showed the strongest correlation with the expression of LINC01605 in the GTEx dataset and the TCGA dataset. While most of the identified genes had distinct expression levels in ESCC tissues with high LINC01605 expression compared with ESCC tissues with low LINC01605 expression, we identified a group of genes, including *MELK, PTTG1, aurora kinase B (AURKB), BMP7, and AQP3*, whose expression remained unchanged in ESCC tissues with high LINC01605 expression compared with ESCC tissues with low LINC01605 expression (Fig. 3C). Notably, three of these genes (*MELK, PTTG1, and AURKB*) were functionally associated with cell cycle regulation, and their expression was strongly correlated with LINC01605 expression exclusively in normal epithelium. These findings suggest that LINC01605 plays context-dependent roles, operating through divergent pathways in normal versus malignant squamous epithelial cells states. In fact, Cross-dataset analysis revealed that the TOP20 genes most strongly correlated (Pearson $|r| > 0.65$) with LINC01605 in GTEx showed minimal overlap with the TOP20 correlated genes in TCGA. Nevertheless, 75% (15/20) of GTEx-identified TOP20 genes retained statistically significant

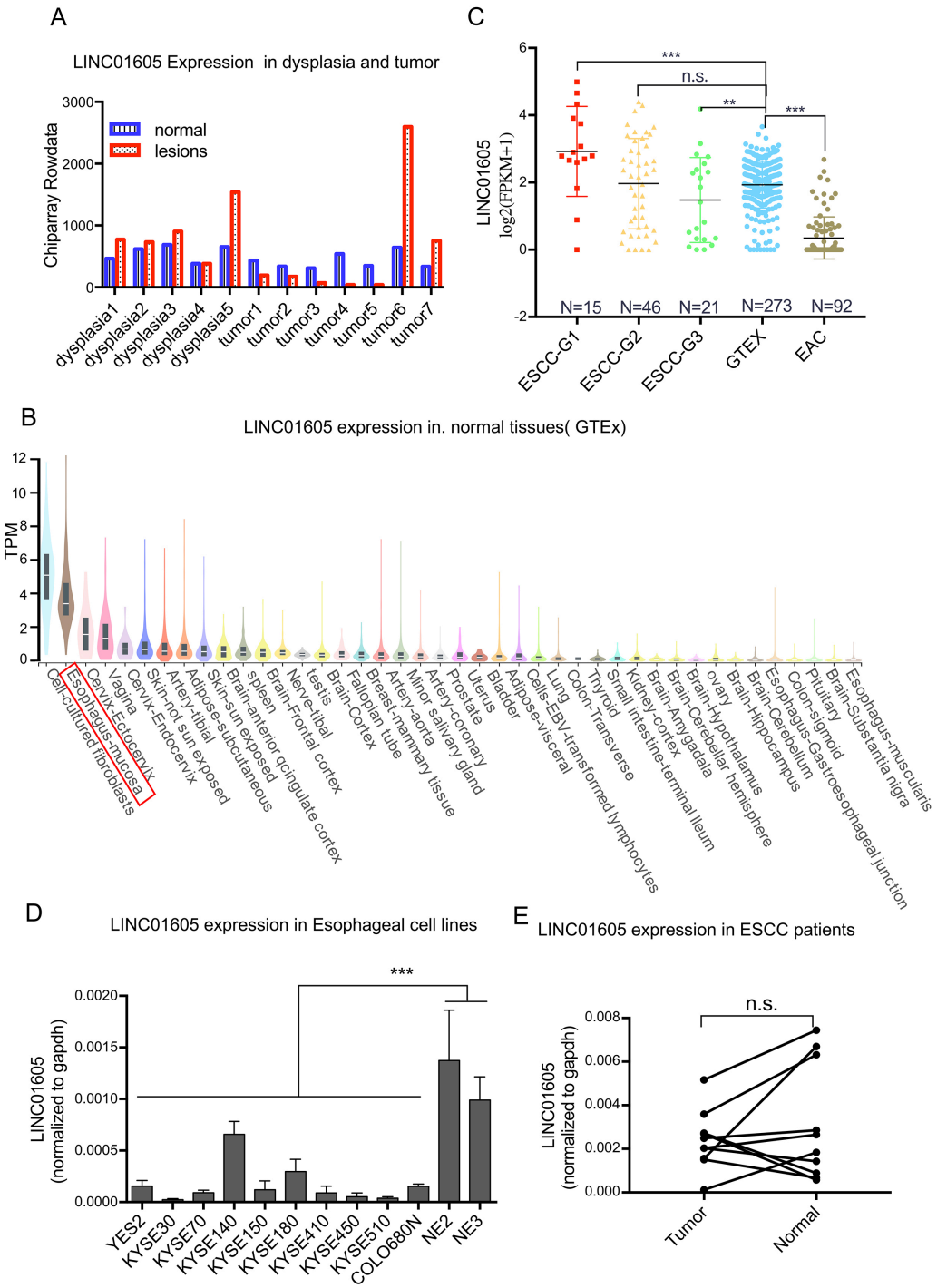

Fig. 2. Expression of LINC01605 in esophageal tissues and cell lines. (A) Expression level of LINC01605 in lesions and paired normal tissues from 5 patients with dysplasia and 7 patients with ESCC as detected by microarrays. (B) The expression levels of LINC01605 across diverse normal tissues in the GTEx database with the top 40 highest-expressing tissue types showed. The red box marked the squamous epithelium of the esophageal mucosa (C). Expression levels of LINC01605 in histological grade 1, 2, and 3 ESCC samples from the TCGA dataset; normal esophageal squamous epithelium samples from the GTEx dataset; and esophageal adenocarcinoma samples from the TCGA dataset. (D) Expression level of LINC01605 in 10 ESCC cell lines and 2 immortalized esophageal epithelial cell lines as determined by qRT-PCR. (E) Expression level of LINC01605 in 10 pairs of ESCC and adjacent normal tissues as determined by qPCR. ESCC-G1/2/3: histological grades of 1, 2, and 3, respectively, ESCC samples from the TCGA dataset; GTEx: normal esophageal squamous epithelium from the GTEx dataset; EAC: esophageal adenocarcinoma from the TCGA dataset. ** $p < 0.01$, *** $p < 0.001$, n.s., $p \geq 0.05$. ESCC, esophageal squamous cell carcinoma; GTEx, Genotype-Tissue Expression Project; TCGA, The Cancer Genome Atlas Program; qRT-PCR, quantitative real-time PCR.

correlations ($p < 0.05$) with LINC01605 in TCGA, despite attenuated correlation strengths (median |r| decrease: 0.3). Conversely, 75% (15/20) of TCGA TOP20 correlates maintained significant associations in GTEx, though with similarly diminished effect sizes. We observed conserved strong correlations with the expression of epidermis development-associated genes, including *KRT5*, *COL17A1*, *KRT14*, *VDR*, and *BNC1*, across both datasets (Fig. 3D). This conserved coexpression network supports the idea that LINC01605 participates in squamous cell differentiation pathways during esophageal carcinogenesis. In addition, genes that are associated with cell proliferation, cellular adhesion, and intermediate filament assembly exhibited strong coexpression patterns with LINC01605 in both normal esophageal epithelium and ESCC. Moreover, some of these genes were involved in two or more of the functions described above (Fig. 3D), suggesting that the LINC01605-related genes may regulate the dedifferentiation process through multiple mechanisms such as cell proliferation, adhesion, and movement.

3.4 An In Vitro Study Confirmed That LINC01605 Affects the Proliferation and Migration of Esophageal Squamous Cell Carcinoma Cells

To investigate the phenotypic impact of LINC01605, we performed experiments with the NE3 and KYSE180 cell lines. The NE3 cell line is a normal immortalized esophageal epithelial cell line exhibiting physiologically high LINC01605 expression. This makes this cell line ideal for modeling LINC01605 *loss* during carcinogenesis and avoiding biologically incongruent overexpression. Among esophageal cell lines, KYSE180 cells exhibit moderate LINC01605 expression, allowing the confirmation of both loss- and gain-of-function phenotypes within the same neoplastic context. We transiently knocked down LINC01605 expression in NE3 cells with relatively high endogenous LINC01605 expression and in KYSE180 cells with moderate endogenous LINC01605 expression. Two independent siRNAs (si-1006 and si-1349) efficiently silenced LINC01605 expression in both cell lines (**Supplementary Fig. 1A,B**). The knockdown of LINC01605 increased the proliferation rates of both NE3 and KYSE180 cells, as shown by CCK-8 assays or real-time monitoring of growth. Real-time monitoring data from the xCELLigence Real-Time Cell Analyzer [19,20] revealed distinct separation of the growth curves between the two knockdown KYSE180 cell lines and the control KYSE180 cell line, demonstrating consistent suppression of proliferative capacity throughout the observation period (Fig. 4A, **Supplementary Fig. 2**). The Mann–Whitney U test was performed to analyze the ODs in the NE3 cells between the si-1006/si-1349 and si-NC groups at each time point. Significant differences ($p < 0.05$) were observed beginning at 48 hrs (Fig. 4B). Moreover, Transwell experiments revealed that the migration of the two cell lines was significantly greater after LINC01605 knockdown, and the number of cells that migrated to the lower chambers was significantly greater ($p < 0.001$) than that in the control group (Fig. 4C). In particular, knockdown of LINC01605 in NE3 cells, which mimics the changes in LINC01605 expression that are observed during esophageal squamous epithelial carcinogenesis, indicates that LINC01605 can inhibit proliferation and migration during esophageal squamous epithelial carcinogenesis.

We also attempted to overexpress LINC01605. Although the transcripts of LINC01605 were recorded in Refseq, database mining in LNCpedia [21] revealed >10 overlapping transcripts spanning the LINC01605 locus, suggesting that this transcript undergoes extensive alternative splicing. To confirm the transcript of this lncRNA that is found in esophageal cell lines, we designed primers according to the NR_121620.2 transcript and carried out RACE experiments in NE3 cells. We identified three distinct termination sites in 3′RACE and five initiation variants in 5′RACE. Full-length PCR amplification combining these termini yielded four stable transcripts (**Supplementary Fig. 3**). All 4 variants shared a conserved 3′ terminus but exhibit three alternative 5′ ends. The shortest isoform (named 15.3.1, 985 bp) was fully nested within the longest transcript (named 11.2, 1391 bp). The probe sequence of LINC01605 in our microarray also precisely mapped to overlapping regions. Two 5′ termini and three 3′ ends failed to generate full-length products, likely due to low-abundance transcripts being below detection thresholds.

We constructed overexpression vectors for the longest and shortest LINC01605 transcripts that were identified above and transfected them into KYSE180 cells with moderate endogenous LINC01605 expression and into KYSE30 cells with low endogenous expression; the latter cell type provided a null background system for clean observation of functional restoration following LINC01605 overexpression. Both isoforms were successfully overexpressed in the target cells (**Supplementary Fig. 1C,D**). Functional characterization demonstrated conserved tumor-suppressive effects across isoforms. CCK-8 assays revealed a significant reduction ($p < 0.05$) in the proliferation rates of both KYSE180 and KYSE30 cells overexpressing either transcript when Mann–Whitney U tests were conducted (Fig. 5A,B). Transwell assays revealed 3–10-fold decreases in the number of migrated cells (Fig. 5C). Notably, KYSE30 cells, which exhibit extremely low endogenous LINC01605 expression, displayed profound phenotypic suppression after LINC01605 overexpression. Furthermore, flow cytometry analysis of KYSE30 cells overexpressing either isoform of LINC01605 revealed cell cycle arrest in the G0 phase (**Supplementary Fig. 4**); these results recapitulated the terminal differentiation-associated cell cycle exit that is observed in normal squamous epithelium.

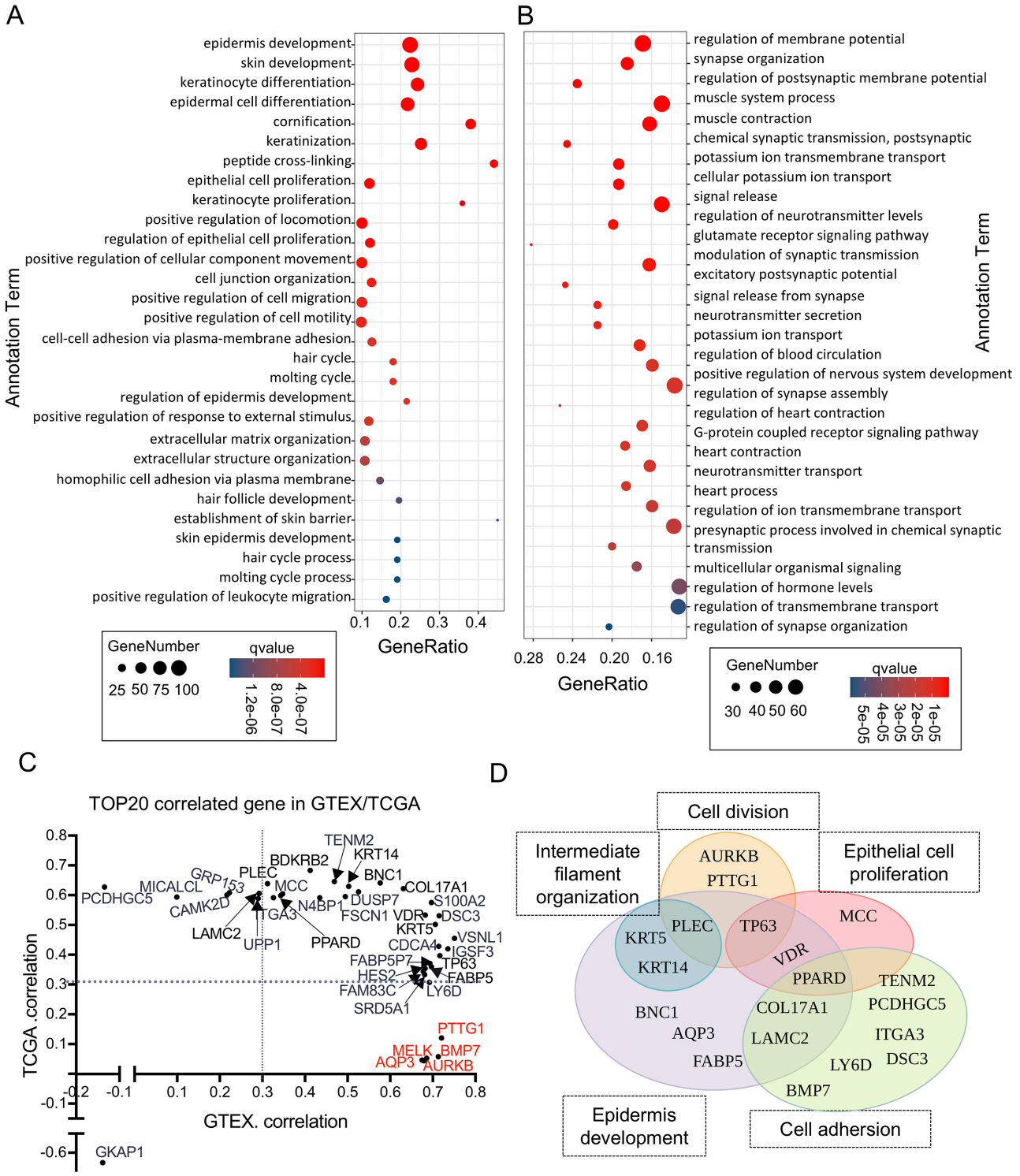

Fig. 3. The functions of LINC01605 are explained by covariant genes and coexpressed genes. (A) Representative GO biological process (BP) terms of the genes whose expression was lower in samples with low LINC01605 expression. (B) Representative GO BP terms of the genes whose expression was higher in samples with low LINC01605 expression. (C) The top 20 genes related to the expression of LINC01605 in the GTEx or TCGA datasets. The X-axis represents the Pearson correlation coefficient with LINC01605 in the GTEx dataset, and the Y-axis represents the Pearson correlation coefficient with LINC01605 in the TCGA dataset. Red represents the genes with no difference in expression levels between tissues with high and low LINC01605 expression. The points indicated by the arrow corresponds to the location of the genes. (D) The functions of the top 20 genes related to LINC01605 in the GTEx or TCGA dataset. GO, gene ontology.

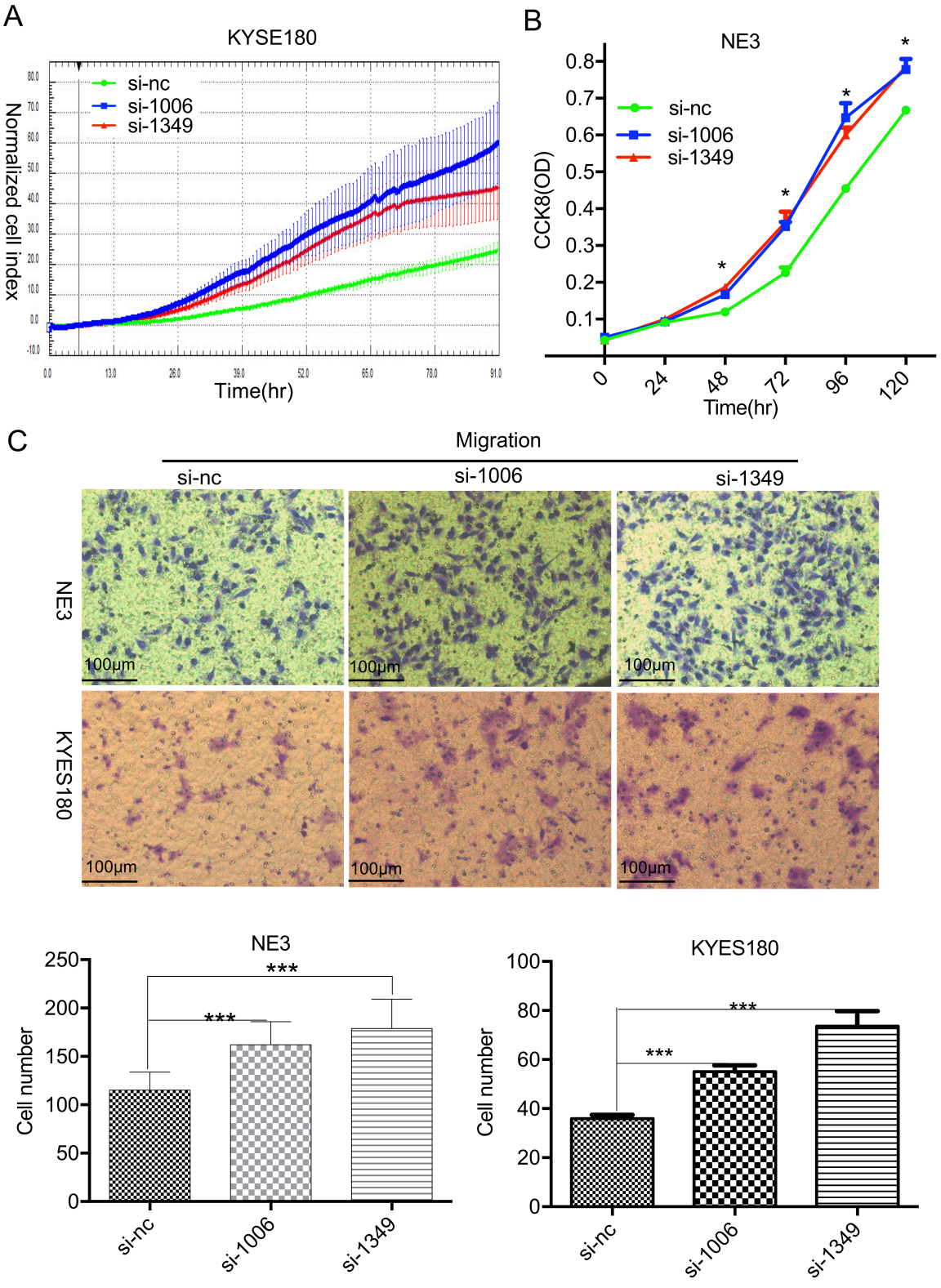

Fig. 4. LINC01605 knockdown promotes the proliferation and migration of KYSE180 and NE3 cells. (A) Growth curve showing cell proliferation after LINC01605 was knocked down in KYSE180 cells. (B) Growth curve showing cell proliferation after LINC01605 was knocked down in NE3 cells. (C) Transwell migration assay showing cell migration after LINC01605 was knocked down in KYSE180 and NE3 cells. Top, representative illustration of migrated cells. Scale bar = 100 μm; bottom, the number of cells that migrated to the lower chamber. si-1006 and si-1349: two distinct siRNAs targeting LINC01065; si-NC: negative control. * $p < 0.05$, *** $p < 0.001$. KYSE180, ESCC cell line; NE3, immortalized normal esophageal mucosal cell line.

3.5 HNRNPC and AURKB are Potential Interactors of LINC01605 Identified by RNA Pull Down Assay

RNA–protein interactions represent a key mechanism by which lncRNAs regulate cellular processes. To identify functional partners of LINC01605, we performed RNA pull-down assays in NE3 cell lysates, using the two isoforms transcribed *in vitro*, with antisense strands and no RNA systems used as negative controls. Two distinct protein bands within the 30–40 kDa range were selectively enriched by both isoforms compared with antisense controls and noRNA controls by two independent pull down assays (Fig. 6A, **Supplementary Fig. 5**). Mass spectrometry analysis of these differential bands revealed that heterogeneous nuclear ribonucleoprotein C (HNRNPC) was the predominant interactor, with the highest scores and sequence coverage across all the proteins identified. Repeat RNA pull-down assays followed by Western blot analysis confirmed significant enrichment of HNRNPC at the expected molecular weight position (35–40 kDa) (Fig. 6B). HNRNPC, which is a known RNA-binding protein that is involved in transcriptional regulation and alternative polyadenylation [22], may mediate the posttranscriptional processing of LINC01605. We interrogated the starBase database for protein-lncRNA interactions, leveraging its comprehensive catalog of lincRNA interactomes derived from high-throughput CLIP-seq assays targeting established RNA-binding proteins [23]. LINC01605 was found to bind HNRNPC in multiple clip-seq experiments (**Supplementary Table 1**). These findings confirm our RNA pull-down data and establish the potential relevance of the HNRNPC-LINC01605 interaction *in vivo*.

In addition to HNPNPC, AURKB was shown to be pulled down by 11.2 and 15.3.1 relative to the antisense control and no RNA control after strict selection of the MS results with Score >5, coverage $\geq 10\%$, unique peptide ≥ 2, and protein molecular weight matching the position of the bands that were sent for testing. AURKB was the most highly enriched protein that was not belonged to a classic RNA-binding protein. Chen B *et al*. [24] reported that the lncRNA CCTA2 could regulate the phosphorylation of AURKB by directly binding to AURKB, indicating the potential RNA-binding capacity of AURKB. Repeat RNA pull-down assays followed by Western blot analysis also confirmed that significant HNRNPC and AURKB enrichment in the LINC01605 RNA complexes relative to negative controls (Fig. 6B). Further, due to the absence of high-throughput interaction data for AURKB-bound lncRNAs, we employed established protein-RNA interaction prediction tools. RPISeq [25] analysis revealed a higher interaction probability between AURKB and LINC01605 (RF classifier score: 0.9) than HNRNPC-LINC01065 (RF classifier score: 0.7–0.8). Using catRAPID [26], we predicted AURKB's potential RNA partners. Although AURKB lacks a canonical RNA-binding domains (RBDs), resulting in low overall binding scores, LINC01605 exhibited a score comparable to the known AURKB-binding RNA CCAT2, with consistent predicted RBDs. AURKB, which is a core constituent of the chromosomal passenger complex (CPC) that is essential for chromosome segregation and cytokinesis, operates by regulating spindle assembly checkpoints [27,28]. The potential interaction between LINC01605 and AURKB suggests a potential involvement of LINC01605 in G2/M phase regulation via spindle assembly checkpoint modulation. However, these findings differ with previous flow cytometry results in KYSE30 cells, where LINC01605 overexpression induced arrest in the G0 phase rather than G2/M-phase perturbations. Notably, AURKB expression was correlated with LINC01605 expression exclusively in normal esophageal epithelium samples but not in ESCC samples (Fig. 3C). We hypothesize that the regulation of the cell cycle by LINC01605 may not be limited to a single stage of the cell cycle, but could involve multiple stages and could be background dependent. The LINC01605-AURKB interaction may mediate homeostatic cell cycle regulation in normal squamous epithelium, which represents one of the mechanisms.

4. Discussion

Multiomics analyses that integrate premalignant lesions provide critical temporal resolution for distinguishing progressive molecular changes that occur during carcinogenesis, surpassing conventional normal-tumor comparisons that conflate cumulative changes. Our multistage transcriptomic dissection of esophageal squamous carcinogenesis elucidates the stepwise acquisition of oncogenic hallmarks. Comparative analysis of high-grade dysplasia versus invasive carcinoma revealed stage-specific molecular reprogramming: progressive downregulation of esophageal morphogenesis regulators alongside coordinated upregulation of regulators of extracellular matrix remodeling, cell adhesion and angiogenesis. These findings are consistent with those of multiomics studies demonstrating that early-stage pathogenesis is driven by epithelial-intrinsic changes followed by late-stage microenvironmental crosstalk activation as critical transition nodes.

In this study, we revealed that LINC01605, which is an esophagus-specific long noncoding RNA, is significantly downregulated in poorly differentiated ESCC through multistage lesion comparative analysis. We systematically elucidated for the first time that LINC01605 participates in the dedifferentiation process during esophageal squamous epithelial carcinogenesis. Bioinformatics analysis revealed a significant correlation between LINC01605 expression levels and pathological differentiation grade in ESCC. Experimental validation using ESCC cell lines and immortalized esophageal mucosal cell lines consistently demonstrated reduced LINC01605 expression in malignant cells. Comparative analysis of high- and low-LINC01605 expression groups in the TCGA-ESCC datasets revealed significant enrichment of coexpressed

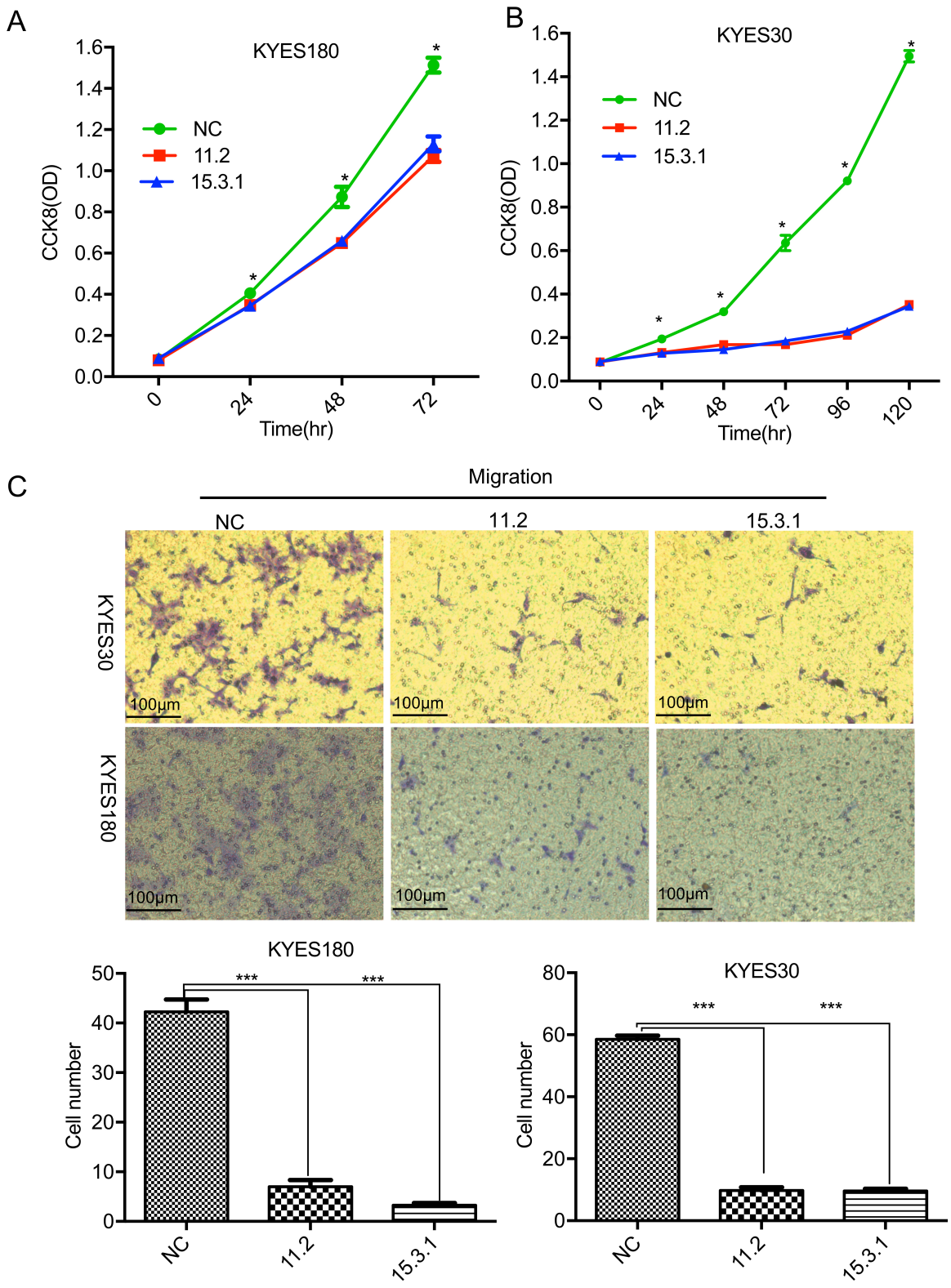

Fig. 5. The overexpression of LINC01605 suppressed the proliferation and migration of KYSE180 and KYSE30 cells *in vitro*. (A) Growth curve showing cell proliferation after LINC01605 was overexpressed in KYSE180 cells. (B) Growth curve showing cell proliferation after LINC01605 was overexpressed in KYSE30 cells. (C) Transwell migration assay showing cell migration after LINC01605 was overexpressed in KYSE180 and KYSE30 cells. Top, representative illustration of migrated cells. Scale bar = 100 μm; bottom, the number of cells that migrated to the lower chamber. 11.2 and 15.3.1: Plasmids carrying LINC01065 transcripts 11.2 and 15.3.1; NC: empty plasmid. * $p < 0.05$, *** $p < 0.001$. KYSE180 and KYSE30, ESCC cell line.

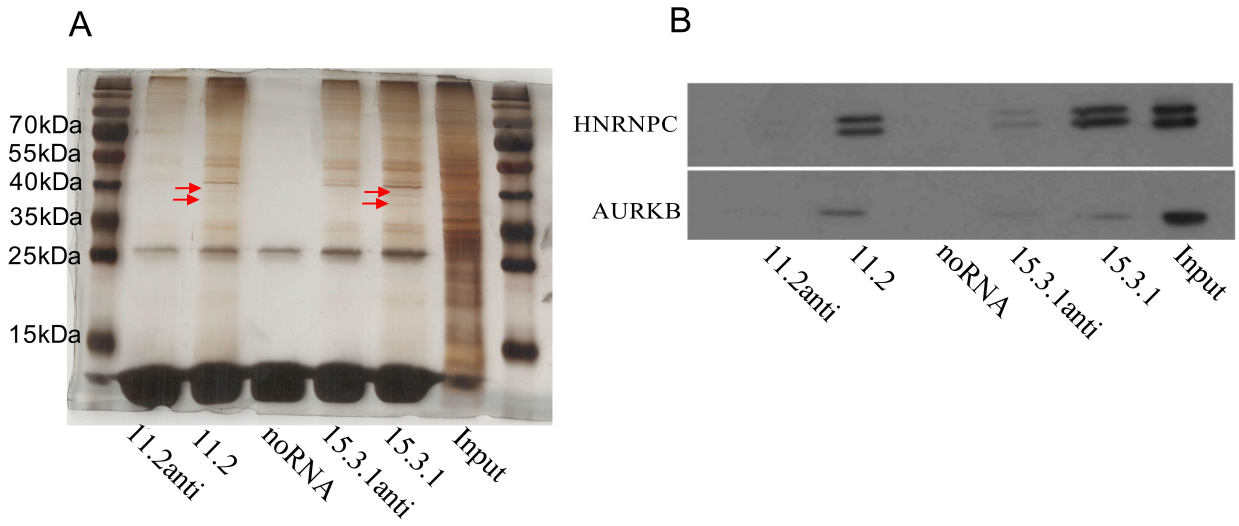

Fig. 6. *In vitro* RNA pull down assays indicated LINC01605 RNA interacts with HNRNPC, AURKB. (A) Image of a silver-stained gel showing bands relative to the protein that specifically binds LINC01605 compared with its antisense RNA; the red arrows indicate the positions of the distinctive bands relative to the control. (B) Western blot of RNA pull-down products showing that HNRNPC and AURKB interact with LINC01605 in esophageal cells. HNRNPC, heterogeneous nuclear ribonucleoprotein C; AURKB, aurora kinase B.

genes in biological processes that are related to esophageal epithelial development and keratinocyte differentiation. Importantly, while previous studies have established the crucial role of dedifferentiation in esophageal carcinogenesis, our work further examined the specific regulatory effects of LINC01605 on maintaining squamous epithelial cell phenotypes. Through gain-of-function and loss-of-function experiments in three cell lines with distinct LINC01605 expression levels, we demonstrated that this gene significantly inhibits the proliferation and migration of esophageal squamous carcinoma cells. These phenotypic observations are consistent with the results of bioinformatics analyses showing distinct biological process activation in ESCC samples with different LINC01605 expression levels, particularly in epithelial cell proliferation and migration. Furthermore, we revealed that LINC01605 overexpression induces tumor cell cycle arrest at the G0 phase, which is a phenomenon that resembles terminal differentiation phenotypes in normal squamous epithelial cells.

However, the limited availability of clinical samples restricted our initial expression profiling to a relatively small sample size, which may have introduced potential bias in detecting subtle changes in gene expression. While this limitation is partially mitigated by the observed consistency with multistage transcriptomic datasets that faithfully recapitulate stepwise changes that occur during esophageal squamous carcinogenesis, the limited cohort size remains a methodological constraint. Although we identified LINC01605 as a critical regulator of esophageal dedifferentiation processes during carcinogenesis, its expression patterns lack sufficient diagnostic specificity, and thus, it cannot serve as a reliable biomarker for detecting malignant transformation in precancerous lesions.

Notably, in contrast to our findings, single-study reports have documented the oncogenic properties of LINC01605 across various malignancies, including clear cell renal carcinoma [29], pancreatic adenocarcinoma [30], cervical cancer [31], ovarian cancer [32], triple-negative breast cancer [33], colorectal carcinoma [34], laryngeal squamous cell carcinoma [35], and nasopharyngeal carcinoma [36]. This tissue-specific differences in function may occur due to several mechanistic considerations. Primarily, our study revealed that LINC01605 expression is highly tissue-specific and restricted to the esophageal squamous epithelium, with negligible LINC01605 expression detected in other epithelial tissues. Genes whose expression demonstrates such pronounced tissue specificity frequently play pivotal roles in organismal pathophysiology and disease progression, likely governed by distinct tissue-specific regulatory networks that may result in divergent functional outcomes across different malignancies [37]. Second, our systematic analysis revealed that LINC01605 participated in multiple cellular activities through diverse upstream/downstream regulatory networks. The protein-coding genes that interact with LINC01605 demonstrate substantial functional heterogeneity, which is consistent with previous reports that described various mechanistic roles across cancer types. The mechanisms by which LINC01605 functions in various cancer types are also very diverse. LINC01605 has been reported to participate in metabolic regulation in pancreatic adenocarcinoma [31], clear cell renal carcinoma [29], and triple-negative breast cancer [33]; act as a competitive endoge-

nous RNA (ceRNA) of some microRNAs in cervical [31] and nasopharyngeal carcinomas [36]; mediate Spectrin Beta, Non-Erythrocytic 2 (SPTBN2) methylation by binding to methyltransferase like 3 (MELLT3) in colorectal carcinoma [34]; and play a role as a mutp53 downstream effector gene in ovarian cancer [32]. This cancer type-specific mechanistic diversity may collectively account for the functional differences observed between ESCC and other tumor types. Finally, LINC01605 exhibits extensive alternative splicing complexity. Currently, genomic databases (Ref-RNA and Ensembl) document more than 100 distinct LINC01605 transcripts and splicing variants; this molecular diversity that has not been systematically addressed in previous functional studies. Notably, previous studies have not comprehensively characterized these transcript-specific isoforms and their potential biological implications. The function and tumor regulatory mechanism of LINC01605 still require more in-depth research. In particular, no reports have been published on the role of LINC01605 in esophageal squamous cell carcinoma thus far.

In this study, through the integrated application of *in vitro* RNA pull-down assays coupled with mass spectrometry and Western blotting validation, we identified LINC01605 interacted with the RNA-binding protein HNRNPC and the cell cycle regulator AURKB. This gives some clue on potential functional partners of LINC01605.

Given the established role of HNRNPC in RNA biogenesis, we hypothesize that HNRNPC may be a potential regulator of LINC01605 transcription, although the potential involvement of this protein in LINC01605 downregulation in ESCC requires further investigation. AURKB, owing to the facts that its expression correlates with that of LINC01605 and that it interacts with LINC1605, may have an upstream or downstream regulatory relationship with LINC10605 during esophageal cancer transformation. AURKB is crucial for ensuring the correct separation of chromosomes, the activation of mitotic spindle test points, and the successful completion of cytokinesis. AURKB has been suggested to be a key oncogene in many other malignant tumors, and its high expression is often associated with disease progression and poor prognosis [38]. Two previous studies demonstrated that AURKB expression was elevated at the transcription level in ESCC [39,40]. Inhibition of AURKB by kinase inhibitors suppresses the growth of ESCC cells and leads to cell cycle arrest in the G2/M phase [41], suggesting that AURKB plays an oncogenic role in ESCC. However, no in-depth research has been conducted to elucidate the specific mechanism by which AURKB participates in esophageal carcinogenesis. Our findings indicate that the interaction between LINC01605 and AURKB potentially represents one way in which LINC01605 functions, but how the LINC10605-AURKB interaction participates in the regulation of esophageal cancer transformation is still unclear.

Concurrently, several unresolved questions persist. RNA pull-down assays, conducted *in vitro* under non-physiological conditions, have inherent limitations: they cannot distinguish direct RNA-protein binding from indirect interactions mediated by co-factors, nor confirm whether such interactions persist in cellular contexts. Therefore, orthogonal validation using *in vivo* techniques—such as RIP (RNA Immunoprecipitation) or CLIP-seq (Cross-Linking Immunoprecipitation Sequencing)—is essential to verify the physiological relevance of interactions between LINC01605 and HNRNPC and AURKB. The expression levels of LINC01605 and AURKB were correlated exclusively in normal esophageal tissues and not in neoplastic tissues. While AURKB was shown to primarily regulate G2/M phase progression in previous reports, LINC01605 overexpression induced arrest in the G0/G1 phase in KYSE30 cells. These suggest that LINC01605 and AURKB may function in a cell context-dependent or cell cycle phases-dependent way, awaiting further exploration with *in situ* technologies. Moreover, RNA pull-down data only confirmed the binding of AURKB but revealed no migration/differentiation-related partners, while transcriptomic analyses revealed that genes whose expression was correlated with LINC01605 expression in normal vs. tumor tissues exhibited divergent functional enrichment. This finding suggests that LINC01605 operates within a complex regulatory network in which AURKB represents only one of several effectors. We may have not yet elucidated the central regulatory mechanism that regulate the multifaceted roles of LINC01605, particularly how its diverse molecular interactions converge to drive phenotypic outcomes. While this study confirms LINC01605's tumor-suppressive role, its molecular mechanisms require further investigation. Ongoing multi-omics and functional studies will address this gap.

5. Conclusion

Our systematic analysis delineates the stepwise acquisition of canonical cancer hallmarks during esophageal squamous carcinogenesis. LINC01605 expression is downregulated during dedifferentiation-associated malignant progression in ESCC, which modulates multiple dedifferentiation-associated phenotypes and promotes cell proliferation and migration. The physical interaction between LINC01605 and AURKB is one potential mechanism underlying the cell cycle-regulatory functions of LINC01605 in esophageal epithelial transformation.

Availability of Data and Materials

The datasets used and analyzed during the current study are available from the corresponding authors on reasonable request.

Author Contributions

SC and XC were responsible for experimental design. XC were responsible for experimental procedures, data analysis, and figures/charts preparation. XH conducted sample collection and chip array detection. XC drafted the initial manuscript and participated in revisions. LF, TX participated in experimental design and manuscript polishing. HA, JF and JL assisted in figure/chart preparation and manuscript revisions. All authors contributed to editorial changes in the manuscript. All authors read and approved the final manuscript. All authors have participated sufficiently in the work and agreed to be accountable for all aspects of the work.

Ethics Approval and Consent to Participate

This study was performed in accordance with the Declaration of Helsinki and was approved by the Ethics Committee of National Cancer Center/Cancer Hospital, Chinese Academy of Medical Sciences and Peking Union Medical College (Ethic Approval Number: 23/532-4275;12-71/605), and all of the patients and their guardians provided signed informed consent.

Acknowledgment

We gratefully acknowledge the assistance and instruction from professor Tong Tong and Dan Li of State Key Laboratory of Molecular Oncology, National Cancer Center/National Clinical Research Center for Cancer/Cancer Hospital.

Funding

This work was supported by the National Natural Science Foundation of China (82372718), the National Key R&D Program of China (2023YFC3503205) and the Chinese Academy of Medical Sciences Innovation Fund for Medical Sciences (No. 2023-I2M-2-004).

Conflict of Interest

The authors declare no conflict of interest.

Supplementary Material

Supplementary material associated with this article can be found, in the online version, at https://doi.org/10.31083/FBL42805.

References

[1] Mao YS, Gao SG, Wang Q, Shi XT, Li Y, Gao WW, *et al*. Epidemiological characteristic and current status of surgical treatment for esophageal cancer by analysis of national registry database. Zhonghua Zhong Liu Za Zhi. 2020; 42: 228–233. (In Chinese)

[2] He M, Wang Z, Lu J, Bai Y, Mao T, Wang J, *et al*. Final analysis of camrelizumab plus chemotherapy for untreated advanced or metastatic esophageal squamous cell carcinoma: The ESCORT-1st trial. Med (New York, N.Y.). 2024; 5: 1137–1149.e3. https://doi.org/10.1016/j.medj.2024.05.008.

[3] Sasaki Y, Tamura M, Koyama R, Nakagaki T, Adachi Y, Tokino T. Genomic characterization of esophageal squamous cell carcinoma: Insights from next-generation sequencing. World Journal of Gastroenterology. 2016; 22: 2284–2293. https://doi.org/10.3748/wjg.v22.i7.2284.

[4] WHO Classification of Tumours Editorial Board. Digestive System Tumours (pp. 30–36). 5th edn. International Agency for Research on Cancer: Lyon, France. 2019.

[5] Liu X, Zhang M, Ying S, Zhang C, Lin R, Zheng J, *et al*. Genetic Alterations in Esophageal Tissues From Squamous Dysplasia to Carcinoma. Gastroenterology. 2017; 153: 166–177. https://doi.org/10.1053/j.gastro.2017.03.033.

[6] Chen XX, Zhong Q, Liu Y, Yan SM, Chen ZH, Jin SZ, *et al*. Genomic comparison of esophageal squamous cell carcinoma and its precursor lesions by multi-region whole-exome sequencing. Nature Communications. 2017; 8: 524. https://doi.org/10.1038/s41467-017-00650-0.

[7] Chang J, Zhao X, Wang Y, Liu T, Zhong C, Lao Y, *et al*. Genomic alterations driving precancerous to cancerous lesions in esophageal cancer development. Cancer Cell. 2023; 41: 2038–2050.e5. https://doi.org/10.1016/j.ccell.2023.11.003.

[8] Chen L, Zhu S, Liu T, Zhao X, Xiang T, Hu X, *et al*. Aberrant epithelial cell interaction promotes esophageal squamous-cell carcinoma development and progression. Signal Transduction and Targeted Therapy. 2023; 8: 453. https://doi.org/10.1038/s41392-023-01710-2.

[9] Chang J, Lu J, Liu Q, Xiang T, Zhang S, Yi Y, *et al*. Single-cell multi-stage spatial evolutional map of esophageal carcinogenesis. Cancer Cell. 2025; 43: 380–397.e7. https://doi.org/10.1016/j.ccell.2025.02.009.

[10] Li R, Li N, Yang Q, Tong X, Wang W, Li C, *et al*. Spatial transcriptome profiling identifies DTX3L and BST2 as key biomarkers in esophageal squamous cell carcinoma tumorigenesis. Genome Medicine. 2024; 16: 148. https://doi.org/10.1186/s13073-024-01422-4.

[11] Plaisier CL, Pan M, Baliga NS. A miRNA-regulatory network explains how dysregulated miRNAs perturb oncogenic processes across diverse cancers. Genome Research. 2012; 22: 2302–2314. https://doi.org/10.1101/gr.133991.111.

[12] Li D, Liu X, Zhou J, Hu J, Zhang D, Liu J, *et al*. Long noncoding RNA HULC modulates the phosphorylation of YB-1 through serving as a scaffold of extracellular signal-regulated kinase and YB-1 to enhance hepatocarcinogenesis. Hepatology (Baltimore, Md.). 2017; 65: 1612–1627. https://doi.org/10.1002/hep.29010.

[13] Hanahan D, Weinberg RA. Hallmarks of cancer: the next generation. Cell. 2011; 144: 646–674. https://doi.org/10.1016/j.cell.2011.02.013.

[14] Hänzelmann S, Castelo R, Guinney J. GSVA: gene set variation analysis for microarray and RNA-seq data. BMC Bioinformatics. 2013; 14: 7. https://doi.org/10.1186/1471-2105-14-7.

[15] Mattick JS, Amaral PP, Carninci P, Carpenter S, Chang HY, Chen LL, *et al*. Long non-coding RNAs: definitions, functions, challenges and recommendations. Nature Reviews. Molecular Cell Biology. 2023; 24: 430–447. https://doi.org/10.1038/s41580-022-00566-8.

[16] Carithers LJ, Ardlie K, Barcus M, Branton PA, Britton A, Buia SA, *et al*. A Novel Approach to High-Quality Postmortem Tissue Procurement: The GTEx Project. Biopreservation and Biobanking. 2015; 13: 311–319. https://doi.org/10.1089/bio.2015.0032.

[17] Kryuchkova-Mostacci N, Robinson-Rechavi M. A benchmark of gene expression tissue-specificity metrics. Briefings in Bioinformatics. 2017; 18: 205–214. https://doi.org/10.1093/bib/bbw008.

[18] Rosekrans SL, Baan B, Muncan V, van den Brink GR. Esophageal development and epithelial homeostasis. American Journal of Physiology. Gastrointestinal and Liver Physiology.

2015; 309: G216–G228. https://doi.org/10.1152/ajpgi.00088.2015.

[19] Song H, Zhao Z, Ma L, Zhao W, Hu Y, Song Y. Novel exosomal circEGFR facilitates triple negative breast cancer autophagy via promoting TFEB nuclear trafficking and modulating miR-224-5p/ATG13/ULK1 feedback loop. Oncogene. 2024; 43: 821–836. https://doi.org/10.1038/s41388-024-02950-4.

[20] Chen D, Zhao Z, Hong R, Yang D, Gong Y, Wu Q, *et al*. Harnessing the FGFR2/NF2/YAP signaling-dependent necroptosis to develop an FGFR2/IL-8 dual blockade therapeutic strategy. Nature Communications. 2025; 16: 4128. https://doi.org/10.1038/s41467-025-59318-9.

[21] Volders PJ, Helsens K, Wang X, Menten B, Martens L, Gevaert K, *et al*. LNCipedia: a database for annotated human lncRNA transcript sequences and structures. Nucleic Acids Research. 2013; 41: D246–D251. https://doi.org/10.1093/nar/gks915.

[22] Fischl H, Neve J, Wang Z, Patel R, Louey A, Tian B, *et al*. hnRNPC regulates cancer-specific alternative cleavage and polyadenylation profiles. Nucleic Acids Research. 2019; 47: 7580–7591. https://doi.org/10.1093/nar/gkz461.

[23] Li JH, Liu S, Zhou H, Qu LH, Yang JH. starBase v2.0: decoding miRNA-ceRNA, miRNA-ncRNA and protein-RNA interaction networks from large-scale CLIP-Seq data. Nucleic Acids Research. 2014; 42: D92–D97. https://doi.org/10.1093/nar/gkt1248.

[24] Chen B, Dragomir MP, Fabris L, Bayraktar R, Knutsen E, Liu X, *et al*. The Long Noncoding RNA CCAT2 Induces Chromosomal Instability Through BOP1-AURKB Signaling. Gastroenterology. 2020; 159: 2146–2162.e33. https://doi.org/10.1053/j.gastro.2020.08.018.

[25] Muppirala UK, Honavar VG, Dobbs D. Predicting RNA-protein interactions using only sequence information. BMC Bioinformatics. 2011; 12: 489. https://doi.org/10.1186/1471-2105-12-489.

[26] Agostini F, Zanzoni A, Klus P, Marchese D, Cirillo D, Tartaglia GG. catRAPID omics: a web server for large-scale prediction of protein-RNA interactions. Bioinformatics (Oxford, England). 2013; 29: 2928–2930. https://doi.org/10.1093/bioinformatics/btt495.

[27] Carmena M, Wheelock M, Funabiki H, Earnshaw WC. The chromosomal passenger complex (CPC): from easy rider to the godfather of mitosis. Nature Reviews. Molecular Cell Biology. 2012; 13: 789–803. https://doi.org/10.1038/nrm3474.

[28] Portella G, Passaro C, Chieffi P. Aurora B: a new prognostic marker and therapeutic target in cancer. Current Medicinal Chemistry. 2011; 18: 482–496. https://doi.org/10.2174/092986711794480203.

[29] Li Y, Hou B, Xu Y, Li H, Zhu Y, Kong C. Comprehensive multi-omics analysis reveals a combination of lncRNAs that synergistically regulate glycolysis and immunotherapeutic effects in renal clear cell carcinoma. Aging. 2024; 16: 11955–11969. https://doi.org/10.18632/aging.206069.

[30] Zhu YH, Jia QY, Yao HF, Duan ZH, Ma XSY, Zheng JH, *et al*. The lncRNA LINC01605 promotes the progression of pancreatic ductal adenocarcinoma by activating the mTOR signaling pathway. Cancer Cell International. 2024; 24: 262. https://doi.org/10.1186/s12935-024-03440-z.

[31] Kong X, Xiong Y, Li L. LINC01605 promotes malignant phenotypes of cervical cancer via miR-149-3p/WNT7B axis. Gene. 2024; 921: 148518. https://doi.org/10.1016/j.gene.2024.148518.

[32] Coan M, Toso M, Cesaratto L, Rigo I, Borgna S, Dalla Pietà A, *et al*. *LINC01605* Is a Novel Target of Mutant p53 in Breast and Ovarian Cancer Cell Lines. International Journal of Molecular Sciences. 2023; 24: 13736. https://doi.org/10.3390/ijms241813736.

[33] Wang W, He X, Wang Y, Liu H, Zhang F, Wu Z, *et al*. LINC01605 promotes aerobic glycolysis through lactate dehydrogenase A in triple-negative breast cancer. Cancer Science. 2022; 113: 2484–2495. https://doi.org/10.1111/cas.15370.

[34] Yue M, Liu T, Yan G, Luo X, Wang L. LINC01605, regulated by the EP300-SMYD2 complex, potentiates the binding between METTL3 and SPTBN2 in colorectal cancer. Cancer Cell International. 2021; 21: 504. https://doi.org/10.1186/s12935-021-02180-8.

[35] Wang XY, Wang L, Xu PC, Huang FJ, Jian X, Wei ZC, *et al*. LINC01605 promotes the proliferation of laryngeal squamous cell carcinoma through targeting miR-493-3p. European Review for Medical and Pharmacological Sciences. 2019; 23: 10379–10386. https://doi.org/10.26355/eurrev_201912_19677.

[36] Zhao W, Xin L, Tang L, Li Y, Li X, Liu R. A positive feedback loop between LINC01605 and NF-κB pathway promotes tumor growth in nasopharyngeal carcinoma. RNA Biology. 2022; 19: 482–495. https://doi.org/10.1080/15476286.2022.2027149.

[37] Greene CS, Krishnan A, Wong AK, Ricciotti E, Zelaya RA, Himmelstein DS, *et al*. Understanding multicellular function and disease with human tissue-specific networks. Nature Genetics. 2015; 47: 569–576. https://doi.org/10.1038/ng.3259.

[38] Tang Z, Li C, Kang B, Gao G, Li C, Zhang Z. GEPIA: a web server for cancer and normal gene expression profiling and interactive analyses. Nucleic Acids Research. 2017; 45: W98–W102. https://doi.org/10.1093/nar/gkx247.

[39] Udhaya Kumar S, Balasundaram A, Anu Preethi V, Chatterjee S, Kameshwari Gollakota GV, Kashyap MK, *et al*. Integrative ontology and pathway-based approach identifies distinct molecular signatures in transcriptomes of esophageal squamous cell carcinoma. Advances in Protein Chemistry and Structural Biology. 2022; 131: 177–206. https://doi.org/10.1016/bs.apcsb.2022.04.003.

[40] Kwon YJ, Lee SJ, Koh JS, Kim SH, Kim YJ, Park JH. Expression patterns of aurora kinase B, heat shock protein 47, and periostin in esophageal squamous cell carcinoma. Oncology Research. 2009; 18: 141–151. https://doi.org/10.3727/096504009790217407.

[41] Yu X, Liang Q, Liu W, Zhou L, Li W, Liu H. Deguelin, an Aurora B Kinase Inhibitor, Exhibits Potent Anti-Tumor Effect in Human Esophageal Squamous Cell Carcinoma. EBioMedicine. 2017; 26: 100–111. https://doi.org/10.1016/j.ebiom.2017.10.030.